Check for updates

Received: 26 October 2022 | Revised: 30 January 2023 | Accepted: 6 February 2023

DOI: 10.1111/jace.19055

Journal of the American Ceramic Society

RAPID COMMUNICATION

Far from equilibrium ultrafast high-temperature sintering of ZrO_2–SiO_2 nanocrystalline glass–ceramics

Le Fu[1] | **Jinghua Wu**[2] | **Sharath Kumar Manjeshwar Sathyanath**[3] | **Bohan Wang**[1] | **Klaus Leifer**[3] | **Håkan Engqvist**[3] | **Salvatore Grasso**[2] | **Wei Xia**[3]

[1]School of Materials Science and Engineering, Central South University, Changsha, China

[2]Key Laboratory of Advanced Technologies of Materials, Ministry of Education, School of Materials Science and Engineering, Southwest Jiaotong University, Chengdu, China

[3]Applied Materials Science, Department of Materials Science and Engineering, Uppsala University, Uppsala, Sweden

Correspondence
Le Fu, School of Materials Science and Engineering, Central South University, 932 Lushan Road, Yuelu District, Changsha 410083, China.
Email: fule2019@csu.edu.cn

Salvatore Grasso, School of Engineering and Materials Science, Queen Mary University of London, Mile End Road, London E1 4NS, UK.
Email: s.grasso@qmul.ac.uk

Wei Xia, Applied Materials Science, Department of Materials Science and Engineering, Uppsala University, Lägerhyddsvägen 1, Uppsala 751 21, Sweden.
Email: wei.xia@angstrom.uu.se

Funding information
National Natural Science Foundation of China, Grant/Award Number: 52102084; Natural Science Foundation of Hunan Province, Grant/Award Number: 2022JJ30718; Swedish Research Council, Grant/Award Number: 2020-04341; Carl Tryggers Foundation, Grant/Award Number: CTS 21:1704; the Swedish Research Council, Grant/Award Numbers: 2019-00207, 2016-05259, 2021-00171

Abstract

Ultrafast high-temperature sintering (UHS) is a novel sintering technique with ultrashort firing cycles (e.g., a few tens of seconds). The feasibility of UHS has been validated on several ceramics and metals; however, its potential in consolidating glass–ceramics has not yet been demonstrated. In this work, an optimized carbon-free UHS was utilized to prepare ZrO_2–SiO_2 nanocrystalline glass–ceramics (NCGCs). The phase composition, grain size, densification behavior, and microstructures of NCGCs prepared by UHS were investigated and compared with those of samples sintered by pressureless sintering. Results showed that NCGCs with a high relative density (~95%) can be obtained within ~50 s discharge time by UHS. The UHS processing not only hindered the formation of $ZrSiO_4$ and cristobalite but also enhanced the stabilization of t-ZrO_2. Meanwhile, owing to the ultrashort firing cycles, the UHS technology allowed the NCGCs to be consolidated in a far from equilibrium state. The NCGCs showed a microstructure of spherical monocrystalline ZrO_2 nanocrystallites embedded in an amorphous SiO_2 matrix.

KEYWORDS
away-from-equilibrium, densification, glass–ceramics, ultrafast high-temperature sintering, ZrO_2–SiO_2

This is an open access article under the terms of the Creative Commons Attribution-NonCommercial-NoDerivs License, which permits use and distribution in any medium, provided the original work is properly cited, the use is non-commercial and no modifications or adaptations are made.
© 2023 The Authors. *Journal of the American Ceramic Society* published by Wiley Periodicals LLC on behalf of American Ceramic Society.

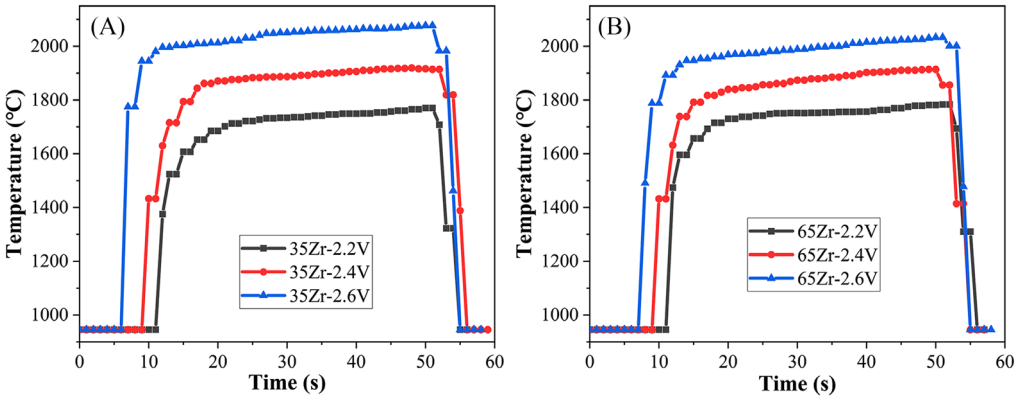

FIGURE 1 The sintering temperature profiles of the 35 mol% ZrO_2–65 mol% SiO_2 samples (A) and the 65 mol% ZrO_2–35 mol% SiO_2 samples (B).

1 | INTRODUCTION

Sintering process conducted by traditional sintering technologies, such as hot-pressing (HP) and hot-isostatic pressing (HIP), is time and energy consuming. This is because the heating rate of HP and HIP techniques is typically in the range of 10–20°C/min. Hence, it requires several hours to consolidate ceramics. The prolonged high-temperature exposure might cause adverse effects on the microstructures of ceramics, such as grain coarsening, undesired chemical reactions, loss of light elements by sublimation, and abnormal grain growth. To overcome these limitations of HP and HIP, in the last decades some innovative sintering routes like SPS,[1] cold sintering,[2] flash sintering (FS),[3] and microwave sintering (MWS)[4] have merged. These sintering routes have significantly promoted the development of sintering technology. However, the pursuit for new sintering techniques never ends. Recently, a novel sintering technique called ultrafast high-temperature sintering (UHS) has been reported.[5] The UHS features ultrahigh heating and cooling rates (up to 10^4°C/min), and high sintering temperatures (up to 3000°C), which shorten the sintering time down to ~10 s.[5]

UHS possesses several readily recognized advantages over the traditional (such as HP, HIP) and the abovementioned relatively-new sintering techniques (such as FS, MWS). First, the ultrashort firing cycle could kinetically retard grain growth. By decreasing the firing schedule to a few seconds, UHS facilitates the preparation of fine-grained ceramics. For instance, Kermani et al.[6] prepared highly dense Al_2O_3 ceramics with a fine grain size of 0.77 μm using UHS, which cannot been achieved by other pressureless sintering (PS) techniques. Second, the ultrafast heating and cooling rates of UHS also notably reduce the volatilization of light elements (Li, Na, etc.) during sintering, which is essential to prepare oxide electrolytes for solid-state batteries.[7–9] Third, the ultrafast heating rate and high temperature promote the materials evolving to a nonequilibrium state, which would possibly bring unexpected benefits, such as reducing activation energy for densification,[10] enhancing,[11] or hindering[12] certain phase transformations.

To date, several materials have been densified using UHS, including oxides,[13] nitrides,[11] and intermetallics.[14] However, to the best of our knowledge, consolidation of glass–ceramics via UHS has not been reported yet. To fill the gap, this study aims to explore the potential of UHS in consolidating ZrO_2–SiO_2 nanocrystalline glass–ceramics (NCGCs). In most of the abovementioned UHS studies, samples were placed between the graphite felt which may cause blackening induced by the carbothermal reduction. To overcome this issue, we employed a newly developed UHS based on tungsten heater,[15] rather than a graphite felt. The novel carbon-free UHS avoids the carbon contamination and carbothermal reduction problems. Different UHS processing conditions were investigated to elucidate the effects of processing conditions on the densification behavior and microstructure of the glass–ceramics.

2 | RESULTS AND DISCUSSIONS

2.1 | UHS heating profiles

Sample designation, chemical composition, and UHS processing parameters are listed in Table S1. The sintering temperature profiles are shown in Figure 1. The temperature reached the 1000°C detection threshold of the pyrometer within 10 s, followed by an ultrafast heating to the dwelling stage with average heating rates of 7000–10 000°C/min (Table S1). During the dwelling stage, the temperature reached a plateau as the electrical power dissipation matched the heat losses by radiation. The UHS

15512916, 2023, 7, Downloaded from https://ceramics.onlinelibrary.wiley.com/doi/10.1111/jace.19055 by Uppsala University Karin Boye, Wiley Online Library on [26/09/2023]. See the Terms and Conditions (https://onlinelibrary.wiley.com/terms-and-conditions) on Wiley Online Library for rules of use; OA articles are governed by the applicable Creative Commons License

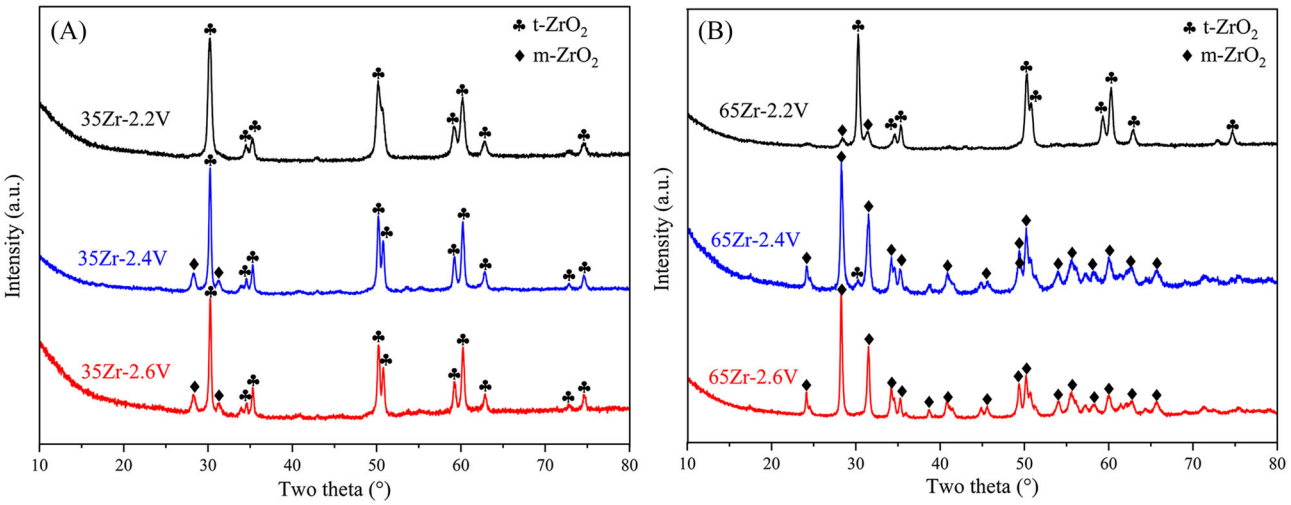

FIGURE 2 XRD patterns of the sintered samples. (A) Samples with the composition of 35 mol% ZrO_2–65 mol% SiO_2. (B) Samples with the composition of 65 mol% ZrO_2–35 mol% SiO_2.

apparatus showed good temperature controllability even at temperature above 2000°C (Figure 1). After the dwelling stage, the electric power was turned off and the samples were rapidly cooled down. From the slope of the curves, the cooling rates were in the range of 7000–10 000°C/min (Figure 1). The entire firing cycles lasted for ~50 s, including heating, dwelling, and cooling steps (Figure 1, Table S1), which was two to three orders of magnitudes shorter than typical firing cycles using either SPS or HP. Hence, the UHS showed obvious advantages in terms of reduction of processing time and consumed energy. All the sintered samples did not experienced blackening, indicating that the novel carbon-free UHS avoids carbon contamination issue.

2.2 | Phase compositions

Both the 35Zr and 65Zr as-calcined powder were amorphous before UHS processing (Figure S1). After UHS processing, the 35Zr-2.2 V sample was purely composed of t-ZrO_2, in comparison, two weak peaks of m-ZrO_2 appeared in the 35Zr-2.4 V sample after sintering at ~1913°C (Figure 2A). Quantitative analysis showed that the 35Zr-2.4 V sample consisted of 33.5 vol% m-ZrO_2 and 66.5 vol% t-ZrO_2 (Table 1). With sintering temperature further increasing to ~2079°C, the content of m-ZrO_2 slightly increased to 37.5 vol% in the 35Zr-2.6 V sample (Table 1). In comparison, 35Zr samples sintered by PS (1200°C) consisted of 100 vol% t-ZrO_2 (Table 1, Figure S2). When the sintering temperature increased to 1500°C, 4.8 vol% $ZrSiO_4$, and 60.4 vol% cristobalite were formed in the 35Zr sample sintered by PS (Table 1, Figure S2). According to the ZrO_2–SiO_2 phase diagram,[16] $ZrSiO_4$ and crystalline SiO_2 would form under equilibrium conditions when cooling the material from elevated temperatures, whereas no $ZrSiO_4$ and crystalline SiO_2 were formed in all the 35Zr samples processed by UHS (Table 1), indicating that UHS processing kinetically hindered the formation of $ZrSiO_4$ and crystallization of SiO_2. The ZrO_2–SiO_2 NCGCs prepared by UHS were in a far away-from-equilibrium state compared with the reference samples prepared by PS and the ZrO_2–SiO_2 phase diagram.[16]

For the 65Zr samples, diffraction peaks of both m-ZrO_2 and t-ZrO_2 were detected in the 65Zr-2.2 V sample (Figure 2B), and the volume percentage of the two phases was 31.5 and 68.5 vol% (Table 1), respectively. A large amount of t-ZrO_2 transformed to m-ZrO_2 in the 65Zr-2.4 V sample, resulting in a formation of 92.0 vol% m-ZrO_2 after sintering at ~1917°C (Table 1). With the sintering temperature further increasing to ~2023°C, only diffraction peaks of m-ZrO_2 were detected in the 65Zr-2.6 V sample (Figure 2B). In comparison, 65Zr samples sintered by PS (1200°C) consisted of 100 vol% t-ZrO_2 (Table 1). However, when the sintering temperature of PS increased to 1500°C, a large amount of $ZrSiO_4$ (56.4 vol%) formed, with t-ZrO_2 content reducing to only 4.9 vol% (Table 1).

Grain size plays an important role in the stability of t-ZrO_2. Although m-ZrO_2 is the thermodynamically stable phase at room temperature, it has been identified a critical crystallite size (dozens of nanometers) below which t-ZrO_2 is more stable than m-ZrO_2.[17,18] Upon heating, the increase in grain size decreased the stability of t-ZrO_2 and enhanced the tetragonal to monoclinic phase transformation during cooling. Hence, for both 35Zr and 65Zr samples, with the increase of sintering temperature the volume fraction of t-ZrO_2 decreased and that of the m-ZrO_2 increased (Table 1). In the present study, no t-ZrO_2 stabilization dopants, such

15512916, 2023, 7, Downloaded from https://ceramics.onlinelibrary.wiley.com/doi/10.1111/jace.19055 by Uppsala University Karin Boye, Wiley Online Library on [26/09/2023]. See the Terms and Conditions (https://onlinelibrary.wiley.com/terms-and-conditions) on Wiley Online Library for rules of use; OA articles are governed by the applicable Creative Commons License

TABLE 1 Average grain size, phase composition, and relative density of the studied samples.

Sample	Grain size (nm)		Phase composition (vol%)	Relative density (%)
	t-ZrO_2	m-ZrO_2		
35Zr-2.2V	22.5	–	100% t-ZrO_2	82.1
35Zr-2.4V	48.7	18.7	66.5% t-ZrO_2 + 33.5% m-ZrO_2	94.8
35Zr-2.6V	53.9	19.4	62.5% t-ZrO_2 + 37.5% m-ZrO_2	95.9
PS-1200[a] (35Zr)	20.2	–	100% t-ZrO_2	82.9
PS-1500[a] (35Zr)	>100	–	34.8% t-ZrO_2 + 4.8% $ZrSiO_4$ + 60.4% cri-SiO_2[b]	98.0
65Zr-2.2V	33.8	12.4	66.5% t-ZrO_2 + 31.5% m-ZrO_2	82.5
65Zr-2.4V	–	33.9	8.0% t-ZrO_2 + 92.0% m-ZrO_2	92.9
65Zr-2.6V	–	57.4	100% m-ZrO_2	93.1
PS-1200[a] (65Zr)	54.6	–	100% t-ZrO_2	88.7
PS-1500[a] (65Zr)	–	48.5	4.9% t-ZrO_2 + 32.2% m-ZrO_2 + 56.4% $ZrSiO_4$ + 6.4% cri-SiO_2[b]	96.2

Abbreviation: PS, pressureless sintering.

[a] The grain size and phase composition of 35Zr samples and 65Zr samples sintered by PS were added for comparison.

[b] Cri-SiO_2 stands for cristobalite.

as Y, were added. In the ZrO_2–SiO_2 material system, stabilization of t-ZrO_2 was achieved by the confining effect of the amorphous SiO_2 component.[19,20] However, the stabilization effect of SiO_2 is proportional to the content of SiO_2 in the ZrO_2–SiO_2 material system.[21] The 35Zr samples (65 mol%) had a higher amount of SiO_2 than that of the 65Zr samples (35 mol%), resulting in a higher stabilization effect. The majority of t-ZrO_2 transformed to m-ZrO_2 or reacted with SiO_2 to form $ZrSiO_4$ after PS at 1500°C (Table 1). In comparison, both the 35Zr-2.6 V sample and the 65Zr-2.2 V sample were predominately composed of t-ZrO_2 (Figure 2 and Table 1), indicating that the rapid firing process (within 50 s) realized by UHS was beneficial to the stabilization of t-ZrO_2. Meanwhile, the UHS processing hindered the formation of $ZrSiO_4$ (Table 1, Figure 2). This is because $ZrSiO_4$ was formed via a solid-state reaction between ZrO_2 and SiO_2 at ~1500°C, and the reaction was a diffusion-controlled process.[22] During the ultrashort firing cycle of UHS (Figure 1), the solid-state reaction was kinetically hindered. Hence, no $ZrSiO_4$ was formed in the NCGCs even after UHS processing at ~2032°C (Figure 2).

2.3 | Grain sizes

The grain sizes of the studied samples are listed in Table 1. The average size of t-ZrO_2 in the 35Zr-2.2 V sample was 22.5 nm, and it increased to 48.7 nm in the 35Zr-2.4 V sample, even though the highest sintering temperature of the 35Zr-2.4 V sample (1913°C) was only 143°C higher than that of the 35Zr-2.2 V sample (1770°C), indicating that the ZrO_2 nanocrystallites had a pronounced tendency to coarsening. The average size of t-ZrO_2 was further increased to 53.9 nm when the highest sintering temperature was increased to 2079°C. For 35Zr samples sintered by PS, the average size of ZrO_2 nanocrystallites was 20.2 nm after sintering at 1200°C and significant coarsening occurred during sintering at 1500°C (over 100 nm). Hence, ultrashort firing cycle of UHS effectively hindered coarsening of ZrO_2 nanocrystallites. Similar grain coarsening behaviors were also found in the 65Zr samples (Table 1), that is, first, ZrO_2 nanocrystallites (m-ZrO_2 instead) rapidly coarsened with the increase of sintering temperature; second, grain size of samples prepared by UHS (33.8 nm) showed smaller than that of samples (54.6 nm) prepared by PS, although sintering temperature of UHS (1782°C) was much higher than that of PS (1500°C). Hence, UHS shows advantages over PS in terms of suppressing coarsening of ZrO_2 nanocrystallites.

2.4 | Densification

SEM observations were conducted on the fracture surfaces of the studied samples to investigate the densification behaviors during UHS. The 35Zr-2.2 V sample consisted of loosely packed irregular particles (Figure 3A, Figure S3c). This surface morphology was also almost the same as that of the 35Zr green body after cold isostatic pressing (CIP) (Figure S3a), indicating that the 35Zr-2.2 V sample had not reached high densification after sintering at ~1770°C. The relative density of the sample was 82.1% (Table 1). With sintering temperature increasing to ~2079°C, significant densification occurred. The relative density of the sintered samples increased with the increase of sintering temperature, reaching 95.9% for the 35Zr-2.6 V sample

15512916, 2023, 7, Downloaded from https://ceramics.onlinelibrary.wiley.com/doi/10.1111/jace.19055 by Uppsala University Karin Boye, Wiley Online Library on [26/09/2023]. See the Terms and Conditions (https://onlinelibrary.wiley.com/terms-and-conditions) on Wiley Online Library for rules of use; OA articles are governed by the applicable Creative Commons License

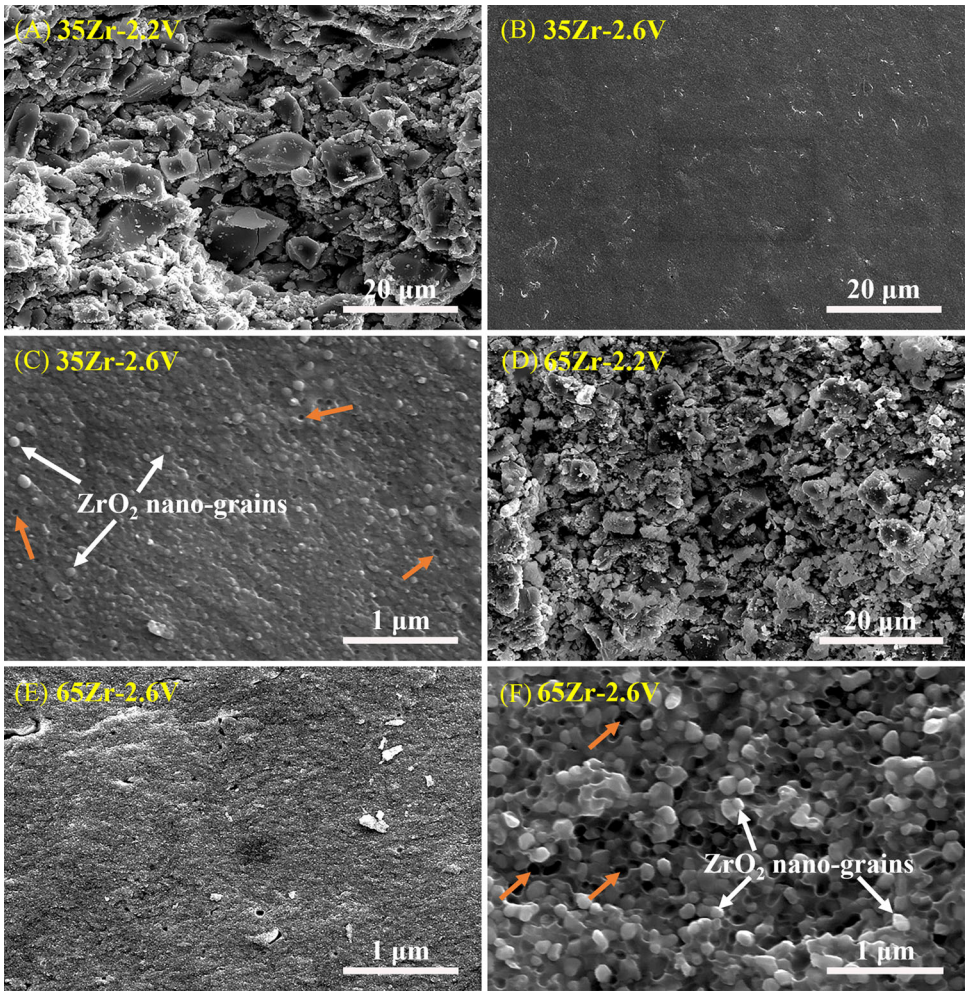

FIGURE 3 Fracture surfaces of the 35Zr sample and the 65Zr sample sintered by ultrafast high-temperature sintering (UHS). (A) 35Zr-2.2 V sample. (B and C) 35Zr-2.6 V sample at low and high magnifications, respectively. (D) 35Zr-2.2 V sample. (E and F) 65Zr-2.6 V sample at low and high magnifications, respectively.

(Table 1). Most parts on the fracture surface showed a smooth morphology (Figure 3B), which is an indicative of high densification. However, several large spherical pores were observed, which were trapped gases due to rapid densification (Figure S3d). There were a large number of spherical ZrO_2 nanocrystallites on the fracture surface (Figure 3C). The 65Zr-2.2 V sample was composed of loosely packed irregular particles (Figure 3D, Figure S3e). The relative density of the 65Zr-2.2 V sample was 82.5% (Table 1). High relative density can be obtained when the sintering temperature reached ~2000°C, being 92.9% and 93.1% for the 65Zr-2.4 V and 65Zr-2.6 V sample (Table 1), respectively. Most parts of the 65Zr-2.6 V sample had been densified (Figure 3E), except that there were some residual pores at some parts (Figure S3f). Meanwhile, spherical ZrO_2 nanocrystallites (white arrows) can be also observed (Figure 3F). Although it is difficult for UHS to reach full densification, it could still achieve high relative density without the application of external pressure, which makes UHS a simpler and cost-effective sintering instrument compared with SPS.

2.5 | Microstructures

The 35Zr-2.6 V sample was selected to conduct TEM observations as it had the highest relative density. In the BF-TEM image (Figure 4A), a lot of spherical and isolated nanocrystallites with dark contrast were observed. The nanocrystallites were embedded in a matrix appeared with bright contrast. The diameter of the nanocrystallites was ~50 nm, which was quite close to the value measured by XRD (Table 1). The nanocrystallites and the matrix demonstrated bright contrast and dark contrast, respectively, in the HAADF-STEM image (Figure 4B), indicating that the nanocrystallites had a heavier average atomic number than that of the matrix. Hence, the nanocrystallites and the matrix were ZrO_2 and SiO_2, respectively. Both the BF-TEM

15512916, 2023, 7, Downloaded from https://ceramics.onlinelibrary.wiley.com/doi/10.1111/jace.19055 by Uppsala University Karin Boye, Wiley Online Library on [26/09/2023]. See the Terms and Conditions (https://onlinelibrary.wiley.com/terms-and-conditions) on Wiley Online Library for rules of use; OA articles are governed by the applicable Creative Commons License

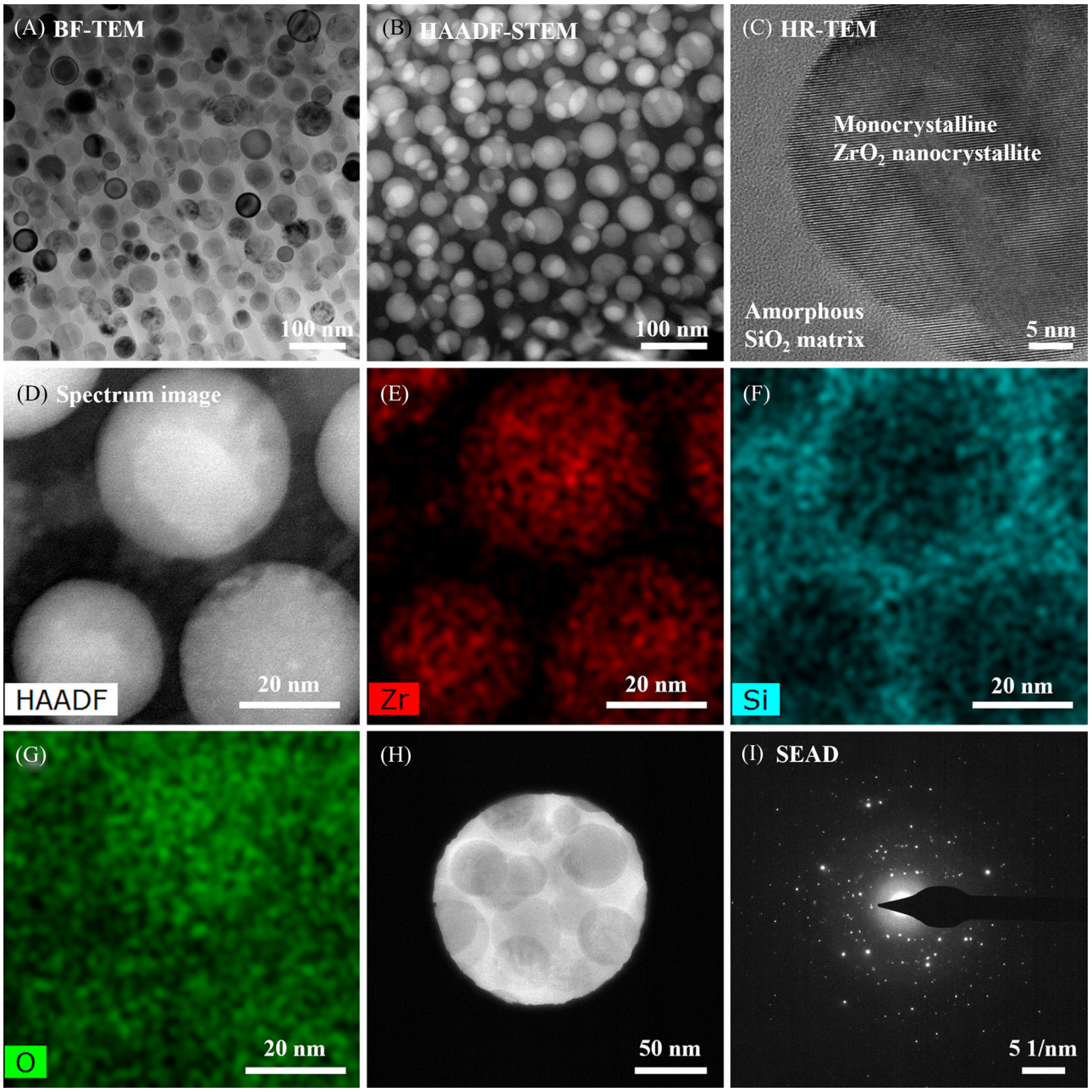

FIGURE 4 TEM and STEM results of the 35Zr-2.6 V sample. (A) BF-TEM image. (B) HAADF-STEM image. (C) HR-TEM image. (D) HAADF-STEM spectrum image. (E–G) Zr map, Si map, and O map, respectively. (H) ZrO_2 nanocrystallites selected by aperture for SEAD analysis. (I) SEAD pattern.

and HAADF-STEM image showed that the ZrO_2 nanocrystallites had a high degree of sphericity. Meanwhile, the ZrO_2 nanocrystallites were isolated by the SiO_2 matrix, as almost no ZrO_2 grain boundaries can be observed. As can be seen from the HR-TEM image (Figure 4C), lattice fringes within in the ZrO_2 nanocrystallite showed the same direction, indicating that the nanocrystallite was a monocrystalline one. No obvious lattice defects were observed within ZrO_2 nanocrystallites although they were formed in an ultrafast firing cycle. Although the ZrO_2 phase ($\sim 9.4 \times 10^{-6}\ C^{-1}$) has much larger coefficient of thermal expansion than that of SiO_2 phase ($\sim 0.5 \times 10^{-6}\ C^{-1}$), no cracking was detected at the heterophase interfaces after experiencing rapid cooling (Figure 4C), which is an important prerequisite for strong bonding between the two phases. The STEM-EDX mapping results (Figure 4D–G) confirmed that the 35Zr-2.6 V sample had a microstructure of ZrO_2 nanocrystallite embedded in a SiO_2 matrix. The

15512916, 2023, 7, Downloaded from https://ceramics.onlinelibrary.wiley.com/doi/10.1111/jace.19055 by Uppsala University Karin Boye, Wiley Online Library on [26/09/2023]. See the Terms and Conditions (https://onlinelibrary.wiley.com/terms-and-conditions) on Wiley Online Library for rules of use; OA articles are governed by the applicable Creative Commons License

SEAD analysis results revealed a polycrystalline nature of the 35Zr-2.6 V sample (Figure 4H,I). We have previously fabricated 35 mol% ZrO_2–65 mol% SiO_2 NCGC by SPS with a heating rate of 100°C/min, a dwelling temperature of ~1200°C, and a dwelling time of 5 min.[23] The microstructure of the SPSed NCGC was almost identical with the 35Zr-2.6 V sample prepared by UHS in this study, that is, consisting of spherical monocrystalline ZrO_2 nanocrystallites embedded in an amorphous SiO_2 matrix. This distinctive microstructure endows the NCGCs with robust mechanical strength and high translucency.[24] The ultrafast firing cycle of UHS does not exert significant influences on the microstructure formation of the ZrO_2–SiO_2 NCGCs. UHS processing shows great potential in fabricating strong and highly-translucent NCGCs.

3 | CONCLUSIONS

In summary, ZrO_2–SiO_2 NCGCs with low and high ZrO_2 contents were consolidated using an optimized carbon-free UHS, and the results were compared with those of the samples prepared by PS. Reproducible experiments were carried out under an average heating rate of 7000–10 000°C/min with good temperature repeatability even at temperature over 2000°C. Compared with PS, the ultrashort firing cycle (within 50 s) of UHS hindered the formation of $ZrSiO_4$ and cristobalite, meanwhile, it was beneficial to the stabilization of t-ZrO_2 phase. The UHS processing allows the consolidation of ZrO_2–SiO_2 NCGCs in a far away-from-equilibrium state. Carbon contamination-free glass–ceramics with high relative density were obtained by UHS without the need for external pressure. The away-from-equilibrium ZrO_2–SiO_2 NCGCs prepared by UHS showed a microstructure of spherical monocrystalline ZrO_2 nanocrystallites embedded in an amorphous SiO_2 matrix. The ZrO_2 nanocrystallites still maintained a fine grain size (~50 nm) even after sintering at ~2000°C. The optimized UHS technique shows great potentials in manufacturing NCGCs.

ACKNOWLEDGMENTS

Dr. Le Fu acknowledges the financial support of National Natural Science Foundation of China (52102084) and Natural Science Foundation of Hunan Province (2022JJ30718). This study is also supported by the Swedish Research Council (2020-04341) and Carl Tryggers Foundation (CTS 21:1704). We acknowledge Myfab Uppsala for providing facilities and experimental support. Myfab is funded by the Swedish Research Council (2019-00207) as a national research infrastructure. K.L. acknowledges generous support from the Swedish Research Council (project no: 2016-05259 and project no: 2021-00171).

ORCID

Le Fu https://orcid.org/0000-0001-6812-1827
Jinghua Wu https://orcid.org/0000-0002-6292-8918
Salvatore Grasso https://orcid.org/0000-0002-2753-4008

REFERENCES

1. Chen F, Yan K, Zhou J, Zhu Y, Hong J. Multilayer graphene and β-Si_3N_4 whisker-reinforced porous Si_3N_4 ceramics by spark plasma incomplete sintering. Mater Sci Eng A. 2021;823:141770. https://doi.org/10.1016/j.msea.2021.141770
2. Guo J, Guo H, Baker AL, Lanagan MT, Kupp ER, Messing GL, et al. Cold sintering: a paradigm shift for processing and integration of ceramics. Angew Chem Int Ed. 2016;55:11457–61. https://doi.org/10.1002/anie.201605443
3. Manière C, Lee G, Olevsky EA. Flash sintering of complex shapes. Appl Mater Today. 2022;26:101293. https://doi.org/10.1016/j.apmt.2021.101293
4. Manshor H, Abdullah EC, Azhar AZA, Sing YW, Ahmad ZA. Microwave sintering of zirconia-toughened alumina (ZTA)-TiO_2-Cr_2O_3 ceramic composite: the effects on microstructure and properties. J Alloys Compd. 2017;722:458–66. https://doi.org/10.1016/j.jallcom.2017.06.115
5. Wang C, Ping W, Bai Q, Cui H, Hensleigh R, Wang R, et al. A general method to synthesize and sinter bulk ceramics in seconds. Science. 2020;368:521–6. https://doi.org/10.1126/science.aaz7681
6. Kermani M, Dong J, Biesuz M, Linx Y, Deng H, Sglavo VM, et al. Ultrafast high-temperature sintering (UHS) of fine grained α-Al_2O_3. J Eur Ceram Soc. 2021;41:6626–33. https://doi.org/10.1016/j.jeurceramsoc.2021.05.056
7. Lin Y, Luo N, Quattrocchi E, Ciucci F, Wu J, Kermani M, et al. Ultrafast high-temperature sintering (UHS) of $Li_{1.3}Al_{0.3}Ti_{1.7}(PO_4)_3$. Ceram Int. 2021;47:21982–7. https://doi.org/10.1016/j.ceramint.2021.04.216
8. Wang R, Dong Q, Wang C, Hong M, Gao J, Xie H, et al. High-temperature ultrafast sintering: exploiting a new kinetic region to fabricate porous solid-state electrolyte scaffolds. Adv Mater. 2021;33:2100726. https://doi.org/10.1002/adma.202100726
9. Hong M, Dong Q, Xie H, Clifford BC, Qian J, Wang X, et al. Ultrafast sintering of solid-state electrolytes with volatile fillers. ACS Energy Lett. 2021;6:3753–60.
10. Dong J, Pouchly V, Biesuz M, Tyrpekl V, Vilémová M, Kermani M, et al. Thermally-insulated ultra-fast high temperature sintering (UHS) of zirconia: a master sintering curve analysis. Scr Mater. 2021;203:114076. https://doi.org/10.1016/j.scriptamat.2021.114076
11. Luo RX, Kermani M, Guo ZL, Dong J, Hu CF, Zuo F, et al. Ultrafast high-temperature sintering of silicon nitride: a comparison with the state-of-the-art techniques. J Eur Ceram Soc. 2021;41:6338–45. https://doi.org/10.1016/j.jeurceramsoc.2021.06.021
12. Biesuz M, Galotta A, Motta A, Kermani M, Grasso S, Vontorová J, et al. Speedy bioceramics: rapid densification of tricalcium phosphate by ultrafast high-temperature sintering. Mater Sci Eng C. 2021;127:2–10. https://doi.org/10.1016/j.msec.2021.112246
13. Guo RF, Mao HR, Zhao ZT, Shen P. Ultrafast high-temperature sintering of bulk oxides. Scr Mater. 2021;193:103–7. https://doi.org/10.1016/j.scriptamat.2020.10.045

15512916, 2023, 7, Downloaded from https://ceramics.onlinelibrary.wiley.com/doi/10.1111/jace.19055 by Uppsala University Karin Boye, Wiley Online Library on [26/09/2023]. See the Terms and Conditions (https://onlinelibrary.wiley.com/terms-and-conditions) on Wiley Online Library for rules of use; OA articles are governed by the applicable Creative Commons License

14. Chen G, Wang Y, Wang X, Zhao Y, Dong Q, Hao L, et al. Target-sintering of single-phase bulk intermetallics via a fast-heating-induced rapid interdiffusion mechanism. ACS Mater Lett. 2022;4:480–6.
15. Wu J, kermani M, Zhu D, Li J, Lin Y, Hu C, et al. Carbon free ultra-fast high temperature sintering of translucent zirconia. Scr Mater. 2022;210:114476. https://doi.org/10.1016/j.scriptamat.2021.114476
16. Kim H, McIntyre PC. Spinodal decomposition in amorphous metal-silicate thin films: phase diagram analysis and interface effects on kinetics. J Appl Phys. 2002;92:5094–102. https://doi.org/10.1063/1.1510590
17. Fu L, Li B, Xu G, Huang J, Engqvist H, Xia W. Size-driven phase transformation and microstructure evolution of ZrO_2 nanocrystallites associated with thermal treatments. J Eur Ceram Soc. 2021;41:5624–33. https://doi.org/10.1016/j.jeurceramsoc.2021.04.058
18. Castro RHR. On the thermodynamic stability of nanocrystalline ceramics. Mater Lett. 2013;96:45–56. https://doi.org/10.1016/j.matlet.2013.01.007
19. Vasanthavel S, Derby B, Kannan S. Stabilization of a t-ZrO_2 polymorph in a glassy SiO_2 matrix at elevated temperatures accomplished by ceria additions. Dalton Trans. 2017;46:6884–93. https://doi.org/10.1039/C7DT01225J
20. Del Monte F, Larsen W, Mackenzie JD. Chemical interactions promoting the ZrO_2 tetragonal stabilization in ZrO_2-SiO_2 binary oxides. J Am Ceram Soc. 2000;83:1506–12. https://doi.org/10.1111/j.1151-2916.2000.tb01418.x
21. Monte F, Larsen W, Mackenzie JD. Stabilization of tetragonal ZrO_2 in ZrO_2-SiO_2 binary oxides. J Am Ceram Soc. 2004;83:628–34. https://doi.org/10.1111/j.1151-2916.2000.tb01243.x
22. Wang S, Peng C, Lü M, Wu J. Effect of ZnO on crystallization of zircon from zirconium-based glaze. J Am Ceram Soc. 2013;96:2054–7. https://doi.org/10.1111/jace.12441
23. Fu L, Wu C, Grandfield K, Unosson E, Chang J, Engqvist H, et al. Transparent single crystalline ZrO_2-SiO_2 glass nanoceramic sintered by SPS. J Eur Ceram Soc. 2016;36:3487–94. https://doi.org/10.1016/j.jeurceramsoc.2016.05.016
24. Fu L, Engqvist H, Xia W. Highly translucent and strong ZrO_2-SiO_2 nanocrystalline glass ceramic prepared by sol-gel method and spark plasma sintering with fine 3D microstructure for dental restoration. J Eur Ceram Soc. 2017;37:4067–81. https://doi.org/10.1016/j.jeurceramsoc.2017.05.039

SUPPORTING INFORMATION

Additional supporting information can be found online in the Supporting Information section at the end of this article.

How to cite this article: Fu LE, Wu J, Sathyanath SKM, Wang B, Leifer K, Engqvist H, et al. Far from equilibrium ultrafast high-temperature sintering of ZrO_2–SiO_2 nanocrystalline glass–ceramics. J Am Ceram Soc. 2023;106:4005–4012. https://doi.org/10.1111/jace.19055

15512916, 2023, 7, Downloaded from https://ceramics.onlinelibrary.wiley.com/doi/10.1111/jace.19055 by Uppsala University Karin Boye, Wiley Online Library on [26/09/2023]. See the Terms and Conditions (https://onlinelibrary.wiley.com/terms-and-conditions) on Wiley Online Library for rules of use; OA articles are governed by the applicable Creative Commons License